





Ultrasensitive optomechanical strain sensor

QIANG ZHANG,^{1,2,3}  SIMIN DU,^{1,2} SHIWEI YANG,^{1,2} QUANSEN WANG,^{1,2} JIE ZHANG,^{1,2} DOUDOU WANG,^{1,2} AND YONGMIN LI^{1,2,4} 

¹State Key Laboratory of Quantum Optics and Quantum Optics Devices, Institute of Opto-Electronics, Shanxi University, Taiyuan 030006, China

²Collaborative Innovation Center of Extreme Optics, Shanxi University, Taiyuan, Shanxi 030006, China

³qzhang@sxu.edu.cn

⁴yongmin@sxu.edu.cn

Abstract: We demonstrate an ultrasensitive optomechanical strain sensor based on a SiN membrane and a Fabry-Perot cavity, enabling the measurements of both static and dynamic strain by monitoring reflected light fluctuations using a single-frequency laser. The SiN membrane offers high-quality-factor mechanical resonances that are sensitive to minute strain fluctuations. The two-beam Fabry-Perot cavity is constructed to interrogate the motion state of the SiN membrane. A static strain resolution of 4.00 nε is achieved by measuring mechanical resonance frequency shifts of the SiN membrane. The best dynamic resolution is 4.47 pεHz^{-1/2}, which is close to that of the sensor using high-finesse cavity and optical frequency comb, overcoming the dependence of ultrasensitive strain sensors on narrow-linewidth laser and high-finesse cavity with frequency locking equipment. This work opens up a promising avenue for a new generation of ultrasensitive strain sensors.

© 2024 Optica Publishing Group under the terms of the [Optica Open Access Publishing Agreement](#)

1. Introduction

Optical strain sensors have wide applications in many science and technology fields including geophysics, aerospace industries, rechargeable batteries, oil and gas reservoirs [1–8]. Optical strain sensors could be divided into two types: static strain sensors and dynamic strain sensors. Usually, static strain could be measured by monitoring optical spectrum shifts of optical interferometers using broadband light sources and optical spectrum analyzers [9–18]. Limited by response velocity of optical spectrum analyzers, these sensors are unsuitable for dynamic strain measurements. Dynamic strain measurements can be realized by monitoring optical power fluctuations of optical interferometers with a single-frequency laser. To improve the dynamic strain sensitivity, an efficient approach is to employ high-finesse optical resonant cavities and low-noise narrow-linewidth lasers to replace two-beam interferometers and broadband light sources [1,19]. For example, using a fiber-optic Fabry-Perot (FP) cavity formed by two fiber Bragg gratings and a laser stabilized with an optical frequency comb, an impressive resolution on the order of 10⁻¹³ εHz^{-1/2} has been demonstrated experimentally [1]. However, most of those ultrasensitive dynamic strain sensors based on high-finesse optical resonant cavities are highly dependent on expensive low-noise narrow-linewidth lasers and sophisticated frequency locking equipment such as optical frequency combs or optical ultra-stable cavities, limiting the large-scale commercial applications. Meanwhile, this method is rarely used to detect static strain owing to light intensity noise.

Optomechanics exploring the interaction between light and mechanical resonator offers exciting approaches for precision sensing technologies [20–25]. Many remarkable optomechanical sensors have been proposed to detect various physical parameters [26–41], from displacements with resolution of 10⁻¹⁹ mHz^{-1/2} [26], forces near the standard quantum limit [27], chip-scale ring laser gyroscopes [28], magnetic fields with resolution of 26 pTHz^{-1/2} [29], single

nanoparticle detections [30,31], electrometer with resolution of $1.37 \text{ mV}^2\text{Hz}^{-1/2}$ [32], kHz-precision wavemeter [33], microwave sensor at the sub-photon level [34], ultrasounds dominated by thermal noise [35], torque sensor with resolution of $10^{-29} \text{ NmHz}^{-1/2}$ [36], to vibrational spectroscopy of single cell [37]. Benefiting from the mechanical and optical double resonant enhancement, optomechanical sensing mechanisms offer novel alternative solutions for more practical and efficient ultrasensitive strain measurements. Recently, two optomechanical thermally induced strain sensors have shown unprecedented static sensitivities of 556 (measured value) and 176671 $\text{Hz}/\mu\epsilon$ (simulated value) [42,43], which are far better than that of optical static strain sensors by measuring the optical spectrum shifts. However, their dynamic strain sensitivities have not been discussed. Therefore, measurement of both static and dynamic strain with high sensitivity for single sensor is a major challenge.

In this work, we present an ultrasensitive strain sensor using an optomechanical system based on a FP cavity and a SiN membrane, enabling the measurements of both static and dynamic strain by detecting optical power fluctuations. The SiN membrane with high-quality-factor (Q) mechanical resonances is sensitive to minute strain, and its motion state is monitored by the two-beam FP cavity formed by the end face of an optical fiber and the SiN membrane. The measurement results show that the static strain resolutions of the (1,1), (1,2), and (2,2) modes are 8.04 ne , 5.03 ne , and 4.00 ne . In addition, the dynamic strain can be measured by monitoring the thermal noise and the response of the sensor. The minimum noise equivalent strain (NES) of $4.47 \text{ pHz}^{-1/2}$ is obtained at the (1,1) mode, where both high-finesse optical cavities and frequency locking equipment have not been used in our experiments. In addition, the static and dynamic strain resolutions can be enhanced furtherly by optimizing the parameters of the SiN membrane. Therefore, the proposed optomechanical strain sensor is promising for various practical applications.

2. Principle

Optomechanical systems based on FP cavity and SiN membrane enable the separate optimization of optical cavities and mechanical resonators for both high quality factors, providing a versatile optomechanical platform for fundamental physics and ultrasensitive sensing [44–46]. The working principle of the optomechanical strain sensor is illustrated in Fig. 1(a), where the underlying mechanism is to transfer the minute ambient strain applied to the SiN membrane to the modulation of the FP cavity. As shown in the inset of Fig. 1(a), the SiN membrane (black) is fixed on the lower surface of a PZT ring (light green) that is used to generate minute strain for the sensor. Several adhesives have been tested, and LOCTITE 4210 has better performance than others and is finally used in our experiments. The PZT ring is supported by a cuboid aluminum block (blue) with a 10mm-depth rectangular through groove. The square SiN membrane (NX5050AS, Norcada) used in our experiments has a thickness of 50 nm and side length of 0.5 mm on a 5×5 mm silicon chip with a thickness of 200 μm . The first four mechanical resonant modes of the SiN membrane are shown in Fig. 1(b), and the (1,2) and (2,1) modes are degenerate for perfect square SiN membrane. A FP cavity is constructed by the end face of the optical fiber and the SiN membrane to interrogate of the motion state of the SiN membrane in the inset of Fig. 1(a). Four standard single mode fibers (SMFs) inserted into a ceramic ferrule are used to read out the displacements of different location of the SiN membrane. The optical images of the SiN membrane, PZT, and ceramic ferrule with four optical fibers are shown in Fig. 1(c) and (d), respectively. Figure 1(e) shows the relative location between the fibers and the SiN membrane in our experiments. With intrinsically high tensile stress, the stoichiometric SiN membrane offers high- Q mechanical modes that are sensitive to minute fluctuations of the intrinsic stress. The two-beam FP cavity can detect real-timely the motion state of the SiN membrane. This mechanism enables extraction of the minute strain applied to the SiN membrane.

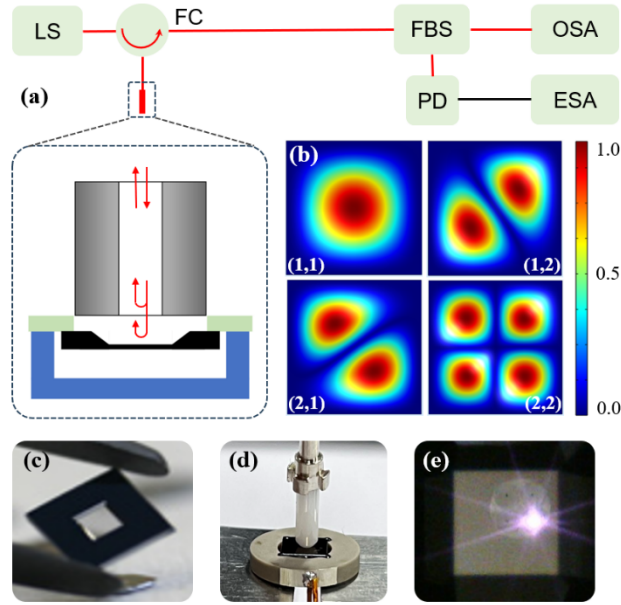


Fig. 1. Design and operating principles of optomechanical strain sensor. (a) Schematic images of experimental apparatus and sensor. (b) Finite-element simulations of the first four mechanical resonant modes of the SiN membrane. (c) and (d) Optical images of the SiN membrane, PZT and ceramic ferrule. (e) Optical image of relative position between the optical fibers and the SiN membrane. LS, light source; FC, fiber circulator; FBS, fiber beam splitter; PD, photodetector; OSA, optical spectrum analyzer; ESA, electrical spectrum analyzer.

The performances of the SiN membrane follow the theoretical model of harmonic oscillators, the mechanical susceptibility $\chi(\omega)$ is given by

$$\chi(\omega) = \frac{1}{\omega_m^2 - \omega^2 + i\omega\omega_m/Q_m} \quad (1)$$

where $\omega_m = 2\pi f_{mn}$ is the resonant angular frequency of the harmonic oscillator, and the resonant frequencies f_{mn} of (m, n) mode is

$$f_{mn}(\varepsilon) = \sqrt{\frac{(\sigma_0 + E\varepsilon)(m^2 + n^2)}{4\rho l^2}} \quad (2)$$

where the σ_0 is the initial tensile stress, E is the Young's modulus, ρ is the mass density, and l is side length of the SiN membrane, respectively. Under resonant exciting ($\omega = \omega_m$), the mechanical susceptibility becomes

$$\chi(\omega_m) = -i \frac{Q_m}{\omega_m^2} \quad (3)$$

When minute strain from the PZT is applied to the SiN membrane, the motion state of the SiN membrane changes and modulates the reflective light of the FP cavity. Therefore, the minute strain is derived from the fluctuation of the reflective light of the FP cavity.

3. Results and discussion

The reflective spectra of the FP cavities are first tested to select the most sensitive laser wavelength for the real-time detection of the motion state of the SiN membrane. Figure 2 shows the reflective

spectra of the FP cavities formed by the three optical fibers and the SiN membrane. In our experiments, a continuous-wave probe light with wavelength of 1550 nm (green dashed line in Fig. 2) is injected into the FP cavity with red reflective spectrum to monitor the SiN membrane. Compared with high-finesse optical cavities, the two-beam FP cavity provides a wider range of line response, relieving the dependence on expensive low-noise narrow-linewidth lasers and sophisticated frequency locking equipment such as optical frequency combs and optical ultra-stable cavities.

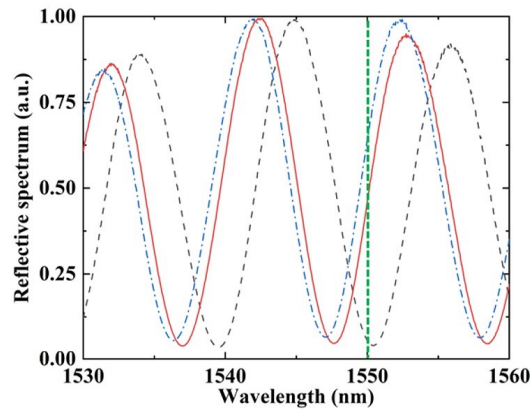


Fig. 2. Reflective spectra of the three FP cavities and wavelength of the probe light (green dashed line).

Figure 3 plots the measured mechanical power spectra of the three resonance modes of the SiN membrane. The black points and red solid curves are the experimental data and the corresponding fitted curves. The resonance frequencies of the three resonant modes are 721.272 kHz, 1139.877 kHz and 1441.978 kHz, and the corresponding Q factors are 3.1×10^5 , 1.1×10^5 , and 2.2×10^5 , respectively. The insets in Fig. 3 are the corresponding vibrating modeshapes.

Static strain was first tested to verify the performance of the sensor. We investigate the resonance frequency shifts of different mechanical modes of the SiN membrane when a static strain is applied to the SiN membrane. Figure 4 plots the calculated and measured resonant frequency shifts of the SiN membrane resonator when the static strain increases from 0 to $50 \mu\epsilon$. According to Eq. (2), the theoretic frequency shifts are inversely proportional to the side length and tensile stress, and are proportional to the mode order (m, n). As shown in Fig. 4(b), the solid lines represent the measured resonance frequency shifts, and the dashed lines are the calculated values, where the ρ and E of SiN are 2700 kg/m^3 and 270 GPa , the σ_0 is 0.705 GPa . The experimental results show that the resonance frequencies increase as the strain increases, and the increasing extents of the high-order modes are larger than that of the low-order modes, which is in good agreement with the theoretic calculated curves. The difference between the experimental and theoretic shifts probably arises from deformation of the glue fixing the SiN membrane to the PZT, and small distinctions between the calculated values and real values of the parameters of the SiN membrane. To remove the influence from the deformation of the glue, we will explore new mounting methods, such as bonding and welding processes. According to the experimental data, the strain sensitivities of the (1,1), (1,2), and (2,2) modes in our experiments are $124.4 \text{ Hz}/\mu\epsilon$, $198.9 \text{ Hz}/\mu\epsilon$, and $250.2 \text{ Hz}/\mu\epsilon$, respectively. The corresponding strain resolutions are up to $8.04 \text{ n}\epsilon$, $5.03 \text{ n}\epsilon$, and $4.00 \text{ n}\epsilon$ for the (1,1), (1,2), and (2,2) modes using an ESA with a RBW of 1 Hz. As far as we know, the maximum wavelength shifts of the two-beam static strain sensors is $102 \text{ pm}/\mu\epsilon$ [16], and the corresponding the strain resolution is $196 \text{ n}\epsilon$ with an OSA (typical resolution 20 pm). Meanwhile, the static strain is obtained by interrogating the resonance frequency shifts

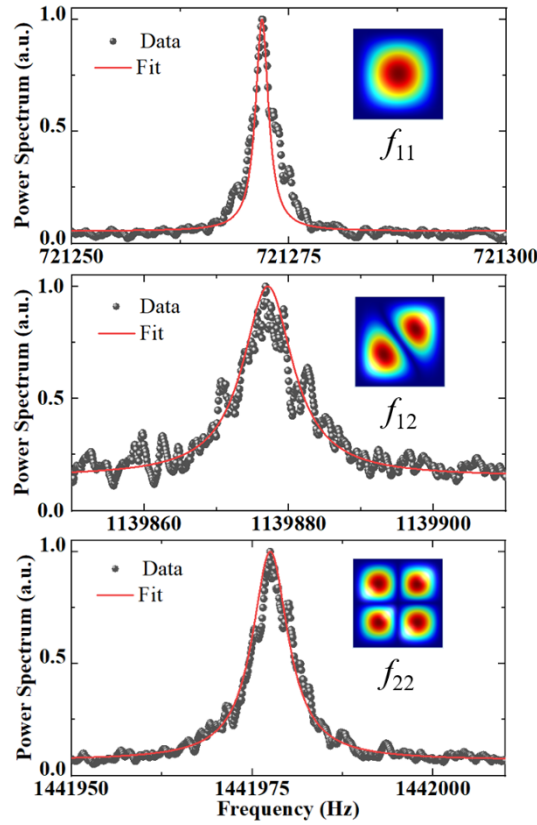


Fig. 3. Normalized mechanical power spectra of the three resonant modes of the SiN membrane. Inset: the corresponding modeshapes.

of mechanical modes of the SiN membrane, alleviating the high stability limit for the intensity and frequency of the laser. Therefore, the proposed optomechanical sensor enables a real-time ultrasensitive static strain detection.

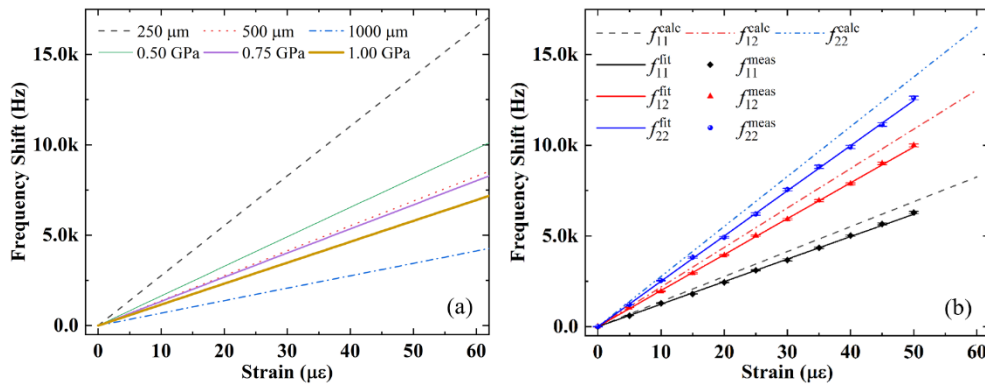


Fig. 4. Mechanical resonance frequency shifts of the SiN membrane as a function of static strain. (a) Responses of the SiN membrane with different side lengths (250, 500, 1000 μm) or tensile stress (0.50, 0.75, 1.00 GPa). (b) Responses of the different mechanical modes.

Next we investigate the response of the proposed sensor to dynamic strain excitation. An arbitrary function generator (AFG3252c, Tektronix) and an ESA (N9010A, Keysight) are used to excite the PZT and analyze the response of the sensor, respectively. The thermal Brownian noises of the (1,1), (1,2), (2,1), and (2,2) mechanical modes are shown in Fig. 5(a), (d) and (g). The signal-to-noise ratios of the (1,1) and (1,2) modes are 20 and 15 dB, respectively, but the (2,1) and (2,2) modes are implicit. Figure 5(b), (e) and (h) show the responses of the sensor as a function of drive frequency of the dynamic strain with a reference constant strain amplitude of 11.1 ne. The (2,1) and (2,2) modes of the SiN membrane are excited and have resonant frequencies of 1141.816 kHz and 1443.527 kHz, respectively. The frequency-dependent noise-equivalent strains (*NES*) of the sensor could be obtained by [1]

$$S^{\min} = \frac{S_{\text{ref}}}{\sqrt{\text{SNR} \times \text{BW}}} \quad (4)$$

where *SNR* is the ratio of the response of the sensor (in Fig. 5(b), (e), and (h)) to the corresponding thermal Brownian noise (in Fig. 5(a), (d), and (g)), *BW* = 10 Hz is the resolution bandwidth of the ESA, and *S*_{ref} is the reference strain. The *NES* of the sensor are shown in Fig. 5(c), (f) and (i). The best strain resolution is 4.47 pεHz^{-1/2} at the fundamental mode of 721.272 kHz. To achieve broadband dynamic strain measurements with resonant sensitivities, the resonant frequencies of the membrane could be swept by some methods, such as temperature control and optical radiation pressure [48,49]. Compared with the sensors [1,19] using low-noise narrow-linewidth lasers and high-finesse optical cavities assisted by sophisticated frequency locking equipment, this work provides an economical and simple ultrasensitive strain sensing technique, overcoming the drawbacks of the pεHz^{-1/2} resolution sensors for practical applications.

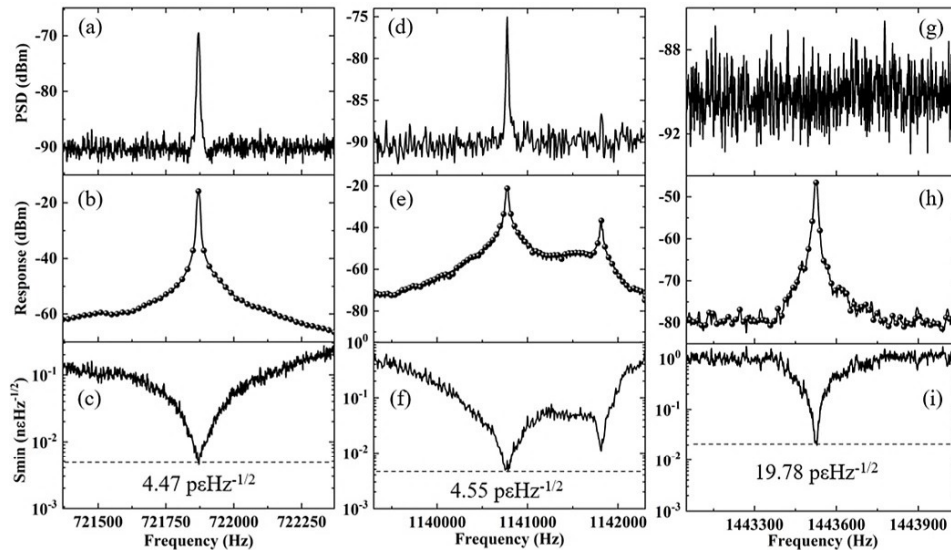


Fig. 5. Experimental results for the optomechanical strain sensor as a function of dynamic strain excitation. (a), (d) and (g) Brownian noise spectra of the four mechanical modes. (b), (e) and (h) Sensor responses of the four mechanical modes. (c), (f) and (i) Strain resolutions of the four mechanical modes.

As shown in Table 1, compared with other optical strain sensors, the proposed sensor enables the measurements of both static and dynamic strain by demodulating the optical power change. The static strain resolution is half of the best measured value in a WGM optomechanical sensor [42]. Meanwhile, the dynamic strain resolution is one order of magnitude lower than the best value

[1,19] without using high-finesse optical cavities and frequency locking equipment, overcoming the dependence of traditional ultrasensitive dynamic strain sensors on high-finesse optical cavities and sophisticated frequency locking equipment. It should be noted the connection method between the sensor and the objects to be monitored needs to be optimized carefully according to the actual ambient conditions, when the proposed sensor is used in practical applications.

Table 1. Summary of optical strain sensors

Optical Cavity		Mechanical Resonator	PDH ⁱ	Static Sensitivity	Dynamic Sensitivity	Reference
Device	Mechanism					
FBG ^a	Multi-beam	No	Yes	N. A.	350feHz ^{-1/2}	[1]
FBG ^a	Multi-beam	No	Yes	N. A.	140feHz ^{-1/2}	[19]
FBG ^a	Multi-beam	No	No	1.16 pm/με	N. A.	[9]
1D PhC ^b	Multi-beam	No	No	0.714 pm*	N. A.	[10]
LPG ^c	Multi-beam	No	No	29.3 pm/με	N. A.	[11]
2D PhC ^b	Multi-beam	Si Cantilever	No	0.95 pm/με	N. A.	[12]
2D PhC ^b	Multi-beam	Si Cantilever	No	132 με	N. A.	[13]
WGM ^d	Multi-beam	SiN Beam	N. A.	556 Hz/με*	N. A.	[42]
FPI ^e	Two-beam	Graphene-Au membrane	No	176671 Hz/με* (simulation)	N. A.	[43]
FPI^e	Two-beam	SiN membrane	No	250.2 Hz/με	4.47 peHz^{-1/2}	This work
MCFI ^f	Two-beam	No	No	1.7 pm/με	N. A.	[14]
OMC ^g	Two-beam	No	No	9.3 pm/με	N. A.	[15]
MZI ^h	Two-beam	No	No	102 pm/με	N. A.	[16]
FPI ^e	Two-beam	No	No	56.69 pm/με	N. A.	[17]
FWM ⁱ	Nonlinear	No	No	4.46 pm/με	N. A.	[47]

^aFBG: fiber Bragg grating

^bPhC: photonic crystal cavity

^cLPG: long-period grating

^dWGM: whispering gallery microcavity

^eFPI: Fabry-Perot interferometer

^fMCFI: multi-core fiber interferometer

^gOMC: microfiber coupler

^hMZI: Mach-Zehnder interferometer

ⁱFWM: four-wave mixing

^jPDH: Pound-Drever-Hall technique

N. A.: not available

*Estimated value from data provided in reference.

The performance of the proposed optomechanical sensor could be optimized furtherly. According to Eq. (2), the resonance frequencies of the mechanical modes of the SiN membrane are proportional to the orders (m,n) of mechanical modes and Young's modulus, and are in inverse proportion to the side length, tensile stress, and the density. Therefore, the static strain resolution could be enhanced by decreasing the side length and tensile stress or choosing high-order modes. In addition, the improvement of the dynamic strain resolution could be obtained by using higher Q_m mechanical resonators. In our experiments, the dynamic strain resolution of 4.47 peHz^{-1/2} is achieved at the fundamental mode of a SiN membrane with Q_m factor of 3.1×10^5 . The mechanical resonators with Q_m factor of 10^8 have been demonstrated experimentally [50,51]. Therefore, the proposed device is a promising candidate for structural engineering, geophysics and aerospace industries.

4. Conclusion

To conclude, we have presented a type of ultrasensitive optical strain sensor using a two-beam FP cavity and SiN membrane optomechanical system, where mechanical resonant enhancement is utilized to improve the sensitivity. By monitoring optical power fluctuations, this sensor could measure both static and dynamic strain, and the static and dynamic strain resolutions are close to the best values of individual static or dynamic strain sensors. The strain resolution of the proposed sensor could be enhanced furtherly by optimizing the SiN mechanical resonator. Our approach provides a promising technique for ultrasensitive strain measurements.

Funding. National Natural Science Foundation of China (11774209, 11804208, 12174232, U21A6006).

Disclosures. The authors declare no conflicts of interest.

Data availability. Data underlying the results presented in this paper are not publicly available at this time but may be obtained from the authors upon reasonable request.

References

1. G. Gagliardi, M. Salza, S. Avino, *et al.*, "Probing the Ultimate Limit of Fiber-Optic Strain Sensing," *Science* **330**(6007), 1081–1084 (2010).
2. N. J. Lindsey, T. C. Dawe, and J. B. Ajo-Franklin, "Illuminating seafloor faults and ocean dynamics with dark fiber distributed acoustic sensing," *Science* **366**(6469), 1103–1107 (2019).
3. C. Lin, Y. Wang, Y. Huang, *et al.*, "Liquid modified photonic crystal fiber for simultaneous temperature and strain measurement," *Photonics Res.* **5**(2), 129–133 (2017).
4. M. Jones, "A sensitive issue," *Nat. Photonics* **2**(3), 153–154 (2008).
5. C. Marques, A. Leal-Júnior, and S. Kumar, "Multifunctional Integration of Optical Fibers and Nanomaterials for Aircraft Systems," *Materials* **16**(4), 1433 (2023).
6. L. Albero Blanquer, F. Marchini, J. R. Seitz, *et al.*, "Optical sensors for operando stress monitoring in lithium-based batteries containing solid-state or liquid electrolytes," *Nat. Commun.* **13**(1), 1153 (2022).
7. M. Niklès and F. Ravet, "Distributed fibre sensors: Depth and sensitivity," *Nat. Photonics* **4**(7), 431–432 (2010).
8. E. Ip, F. Ravet, H. Martins, *et al.*, "Using global existing fiber networks for environmental sensing," *Proc. IEEE* **110**(11), 1853–1888 (2022).
9. C. Chen, A. Laronche, G. Bouwmans, *et al.*, "Sensitivity of photonic crystal fiber modes to temperature, strain and external refractive index," *Opt. Express* **16**(13), 9645–9653 (2008).
10. T. Lu, C. Wu, and P. Lee, "1D photonic crystal strain sensors," *ACS Photonics* **5**(7), 2767–2772 (2018).
11. W. Liu, H. Du, X. Bai, *et al.*, "A S-shaped long-period fiber grating with ultra-high strain sensitivity," *Sens. Actuators, A* **299**, 111614 (2019).
12. B. T. Tung, D. V. Dao, T. Ikeda, *et al.*, "Investigation of strain sensing effect in modified single-defect photonic crystal nanocavity," *Opt. Express* **19**(9), 8821–8829 (2011).
13. C. Lee, J. Thillaiagovindan, C. C. Chen, *et al.*, "Si nanophotonics based cantilever sensor," *Appl. Phys. Lett.* **93**(11), 113113 (2008).
14. J. Villatoro, O. Arrizabalaga, G. Durana, *et al.*, "Accurate strain sensing based on super-mode interference in strongly coupled multi-core optical fibers," *Sci. Rep.* **7**(1), 4451 (2017).
15. L. Zhao, Y. Zhang, Y. Chen, *et al.*, "A fiber strain sensor with high resolution and large measurement scale," *IEEE Sens. J.* **20**(6), 2991–2996 (2020).
16. H. F. Martins, J. Bierlich, K. Wondraczek, *et al.*, "High-sensitivity dispersive Mach-Zehnder interferometer based on a dissimilar-doping dual-core fiber for sensing applications," *Opt. Lett.* **39**(9), 2763–2766 (2014).
17. K. Zhou, M. Z. Ai, Z. H. Qian, *et al.*, "High-sensitivity strain sensor with an in-fiber air-bubble Fabry-Perot interferometer," *Appl. Phys. Lett.* **113**(18), 181901 (2018).
18. C. Zhu, H. Zheng, L. Ma, *et al.*, "Advances in fiber-optic extrinsic Fabry-Perot interferometric physical and mechanical sensors: a review," *IEEE Sens. J.* **23**(7), 6406–6426 (2023).
19. P. Liu, W. Huang, W. Zhang, *et al.*, "Ultrahigh resolution optic fiber strain sensor with a frequency-locked random distributed feedback fiber laser," *Opt. Lett.* **43**(11), 2499–2502 (2018).
20. B. Li, L. Ou, Y. Lei, *et al.*, "Cavity optomechanical sensing," *Nanophotonics* **10**(11), 2799–2832 (2021).
21. J. Xia, Q. Qiao, G. Zhou, *et al.*, "Opto-Mechanical Photonic Crystal Cavities for Sensing Application," *Appl. Sci.* **10**(20), 7080 (2020).
22. X. Liu, W. Liu, Z. Ren, *et al.*, "Progress of optomechanical micro/nano sensors: a review," *Int. J. Optomechanics* **15**(1), 120–159 (2021).
23. P. Bianucci, "Optical Microbottle Resonators for Sensing," *Sensors* **16**(11), 1841 (2016).
24. J. Sandoval, G. Paez, and M. Strojnik, "Optomechanical design of a prism rotator," *Proc. SPIE* **4486**, 170–180 (2002).
25. N. Wu, K. Cui, Q. Xu, *et al.*, "On-chip mechanical exceptional points based on an optomechanical zipper cavity," *Sci. Adv.* **9**(3), eabp8892 (2023).

26. A. Schliesser, G. Anetsberger, R. Rivière, *et al.*, “High-sensitivity monitoring of micromechanical vibration using optical whispering gallery mode resonators,” *New J. Phys.* **10**(9), 095015 (2008).
27. S. Schreppler, N. Spethmann, N. Brahms, *et al.*, “Optically measuring force near the standard quantum limit,” *Science* **344**(6191), 1486–1489 (2014).
28. Y. Lai, M. Suh, Y. Lu, *et al.*, “Earth rotation measured by a chip-scale ring laser gyroscope,” *Nat. Photonics* **14**(6), 345–349 (2020).
29. L. Li, G. Brawley, H. Greenall, *et al.*, “Ultrabroadband and sensitive cavity optomechanical magnetometry,” *Photonics Res.* **8**(7), 1064–1071 (2020).
30. J. Zhu, S. K. Ozdemir, Y. Xiao, *et al.*, “On-chip single nanoparticle detection and sizing by mode splitting in an ultrahigh-Q microresonator,” *Nat. Photonics* **4**(1), 46–49 (2010).
31. Z. Shen, M. Tang, Y. Chen, *et al.*, “Unidirectional emission and nanoparticle detection in a deformed circular square resonator,” *Opt. Express* **29**(2), 1666–1677 (2021).
32. J. Xia, Q. Qiao, H. Sun, *et al.*, “Ultrasensitive nanoscale optomechanical electrometer using photonic crystal cavities,” *Nanophotonics* **11**(8), 1629–1642 (2022).
33. R. Niu, M. Li, S. Wan, *et al.*, “kHz-precision wavemeter based on reconfigurable microsoliton,” *Nat. Commun.* **14**(1), 169 (2023).
34. K. Zhang, F. Bariani, Y. Dong, *et al.*, “Proposal for an Optomechanical Microwave Sensor at the Subphoton Level,” *Phys. Rev. Lett.* **114**(11), 113601 (2015).
35. S. Basiri-Esfahani, A. Armin, S. Forstner, *et al.*, “Precision ultrasound sensing on a chip,” *Nat. Commun.* **10**(1), 132 (2019).
36. T. M. Hoang, Y. Ma, J. Ahn, *et al.*, “Torsional Optomechanics of a Levitated Nonspherical Nanoparticle,” *Phys. Rev. Lett.* **117**(12), 123604 (2016).
37. S. Tang, M. Zhang, J. Sun, *et al.*, “Single-particle photoacoustic vibrational spectroscopy using optical microresonators,” *Nat. Photonics* **17**(11), 951–956 (2023).
38. T. Liu, F. Pagliano, R. V. Veldhoven, *et al.*, “Integrated nano-optomechanical displacement sensor with ultrawide optical bandwidth,” *Nat. Commun.* **11**(1), 2407 (2020).
39. X. Zhang, Y. Yang, H. Bai, *et al.*, “Theoretical aspects and sensing demonstrations of cone-shaped inwall capillary-based microsphere resonators,” *Photonics Res.* **5**(5), 516–520 (2017).
40. S. Xie, A. Sharma, M. Romodina, *et al.*, “Tumbling and anomalous alignment of optically levitated anisotropic microparticles in chiral hollow-core photonic crystal fiber,” *Sci. Adv.* **7**(28), eabf6053 (2021).
41. M. W. Pruessner, T. H. Stievater, J. B. Khurgin, *et al.*, “Integrated waveguide-DBR microcavity opto-mechanical system,” *Opt. Express* **19**(22), 21904–21918 (2011).
42. M. W. Pruessner, D. Park, T. H. Stievater, *et al.*, “Optomechanical Cavities for All-Optical Photothermal Sensing,” *ACS Photonics* **5**(8), 3214–3221 (2018).
43. S. Liu, H. Xiao, Y. Chen, *et al.*, “Nano-Optomechanical Resonators Based on Suspended Graphene for Thermal Stress Sensing,” *Sensors* **22**(23), 9068 (2022).
44. J. D. Thompson, B. M. Zwickl, A. M. Jayich, *et al.*, “Strong dispersive coupling of a high-finesse cavity to a micromechanical membrane,” *Nature* **452**(7183), 72–75 (2008).
45. Q. Zhang, C. Yang, J. Sheng, *et al.*, “Dissipative coupling-induced phonon lasing,” *Proc. Natl. Acad. Sci. U. S. A.* **119**(52), e2207543119 (2022).
46. Z. Li, Q. Zhang, X. You, *et al.*, “Suppression of phonon tunneling losses by microfiber strings for high-Q membrane microresonators,” *Appl. Phys. Lett.* **109**(19), 191903 (2016).
47. B. Gu, W. Yuan, M. H. Frosz, *et al.*, “Nonlinear fiber-optic strain sensor based on four-wave mixing in microstructured optical fiber,” *Opt. Lett.* **37**(5), 794–796 (2012).
48. A. Jöckel, M. T. Rakher, M. Korppi, *et al.*, “Spectroscopy of mechanical dissipation in micro-mechanical membranes,” *Appl. Phys. Lett.* **99**(14), 143109 (2011).
49. E. Gavartin, P. Verlot, and T. J. Kippenberg, “Stabilization of a linear nanomechanical oscillator to its thermodynamic limit,” *Nat. Commun.* **4**(1), 2860 (2013).
50. Y. Tsaturyan, A. Barg, E. Polzik, *et al.*, “Ultrasensitive nanomechanical resonators via soft clamping and dissipation dilution,” *Nat. Nanotechnol.* **12**(8), 776–783 (2017).
51. M. J. Beryehi, A. Arabmoheghi, A. Beccari, *et al.*, “Perimeter Modes of Nanomechanical Resonators Exhibit Quality Factors Exceeding 109 at Room Temperature,” *Phys. Rev. X* **12**(2), 021036 (2022).